Germinal center reentries of BCL2-overexpressing B cells drive follicular lymphoma progression

Stéphanie Sungalee,[1,2,3] Emilie Mamessier,[1,2,3] Ester Morgado,[1,2,3] Emilie Grégoire,[4] Philip Z. Brohawn,[5] Christopher A. Morehouse,[5] Nathalie Jouve,[1,2,3] Céline Monvoisin,[6] Cédric Menard,[6] Guillaume Debroas,[1,2,3] Mustapha Faroudi,[1,2,3] Violaine Mechin,[1,2,3] Jean-Marc Navarro,[1,2,3] Charlotte Drevet,[1,2,3] Franziska C. Eberle,[7] Lionel Chasson,[1,2,3] Fannie Baudimont,[1,2,3] Stéphane J. Mancini,[1,2,3] Julie Tellier,[1,2,3] Jean-Michel Picquenot,[8] Rachel Kelly,[9] Paolo Vineis,[9] Philippe Ruminy,[8] Bruno Chetaille,[10] Elaine S. Jaffe,[7] Claudine Schiff,[1,2,3] Jean Hardwigsen,[4] David A. Tice,[5] Brandon W. Higgs,[5] Karin Tarte,[6] Bertrand Nadel,[1,2,3] and Sandrine Roulland[1,2,3]

[1]Centre d'Immunologie de Marseille Luminy, Aix-Marseille Université, Marseille, France. [2]INSERM U1104, Marseille, France. [3]CNRS UMR7280, Marseille, France. [4]Department of Surgery and Liver Transplantation, AP-HM, Hôpital de la Conception, Marseille, France. [5]MedImmune, Translational Sciences, Gaithersburg, Maryland, USA. [6]INSERM U917, Université de Rennes 1, EFS Bretagne, Rennes, France. [7]Hematopathology Section, Laboratory of Pathology, Center for Cancer Research, National Cancer Institute, Bethesda, Maryland, USA. [8]INSERM U918, Department of Pathology, Centre Henri Becquerel, Rouen, France. [9]MRC-HPA Center for Environment and Health, School of Public Health, Imperial College, London, United Kingdom. [10]Department of Pathology, Institut Paoli-Calmettes, Marseille, France.

It has recently been demonstrated that memory B cells can reenter and reengage germinal center (GC) reactions, opening the possibility that multi-hit lymphomagenesis gradually occurs throughout life during successive immunological challenges. Here, we investigated this scenario in follicular lymphoma (FL), an indolent GC-derived malignancy. We developed a mouse model that recapitulates the FL hallmark t(14;18) translocation, which results in constitutive activation of antiapoptotic protein B cell lymphoma 2 (BCL2) in a subset of B cells, and applied a combination of molecular and immunofluorescence approaches to track normal and t(14;18)+ memory B cells in human and BCL2-overexpressing B cells in murine lymphoid tissues. BCL2-overexpressing B cells required multiple GC transits before acquiring FL-associated developmental arrest and presenting as GC B cells with constitutive activation–induced cytidine deaminase (AID) mutator activity. Moreover, multiple reentries into the GC were necessary for the progression to advanced precursor stages of FL. Together, our results demonstrate that protracted subversion of immune dynamics contributes to early dissemination and progression of t(14;18)+ precursors and shapes the systemic presentation of FL patients.

Introduction

Germinal centers (GCs) represent critical sites within lymphoid tissues, where B cell responses to antigen are amplified and refined through the mechanism of affinity maturation (1). Recently, key dynamic features of the GC emerged from 2-photon intravital imaging studies. Antigen-activated B cells are highly motile and move bidirectionally between the dark and light zones, indicating that repeated cycles of cell proliferation and mutation are a central event of affinity maturation (2, 3). Activated B cells can also colonize preexisting GCs containing B cells specific to unrelated antigens, provided that T cell help is available (4, 5). Furthermore, single clones were found to seed multiple GCs, suggesting the iterative involvement of antigen-experienced cells in GC reactions. Two recent mouse studies provided direct evidence that memory B cells promote the persistence and/or reinitiation of secondary GC reactions following antigen recall (6, 7). Importantly, whereas

switched memory B cells will rapidly undergo clonal expansion and differentiation into high-affinity plasma cells, the IgM subset reenters a GC reaction, allowing the formation of a new generation of IgM- and IgG-expressing cells and providing replenishment of the memory pool.

This property of GC reentry and memory B cell response dynamics has provided new perspectives on the understanding of the early steps governing B cell lymphomagenesis, in particular those originating from GC B cells (5). Due to massive clonal expansion combined with the active error-prone genome-remodeling processes of receptor maturation, GC B cells are at increased risk of genomic instability and lymphomagenesis, and many B cell lymphomas have been shown to derive from the GC (8). As a paradigm of such a process, GC entry of naive B cells with t(14;18)(q32;q21) translocation is assumed to be a key step to follicular lymphoma (FL) genesis by allowing BCL2-driven rescue from apoptosis of B cells with low-affinity receptors and accumulation of developmentally blocked GC B cells with constitutive activation-induced cytidine deaminase (AID) activity (9). This "trapping" of activated GC B cells in the reactive follicle would be a key step to malignant progression, whereby genomic instability enhances the acquisition of complementary oncogenic hits and progressive transformation into overt FL, gradually spreading from the founder follicle to the surrounding ones in the node, then disseminating to distant

lymphoid organs, including BM, to eventually manifest as a systemic disease (10). In this complex cascade of events, 2 potential precursors have been identified: FL in situ (FLIS) cells and FL-like cells (FLLCs). FLIS cells are fortuitous histological findings representing the early steps of GC colonization by BCL2+ B cells. FLIS cells typically present as normal reactive lymph nodes (LNs), albeit containing a few (<50%) BCL2hi/CD10hi GCs (11). Molecular analyses have confirmed the implication of a clonal population of t(14;18)+ B cells. Progression to FL has been observed in less than 5% of FLIS patients over a period ranging from a few months to several years (12). However, the tumor does not systematically manifest at the FLIS anatomical site, indicating a dynamic GC process with dissemination of potent precursors in other tissues and blood (11). FLLCs have been proposed as the circulating counterparts of FLIS (12). Although present in approximately 85% of FL patients, t(14;18) is also detectable at low frequencies (~10^{-6}) in up to 70% of individuals in the normal healthy population (13–15), indicating that ectopic BCL2 expression is necessary but not sufficient for FL development. In such individuals, most circulating t(14;18)+ cells constitute an expanding clonal population of atypical blood B cells that have already transited through the GC and display a combination of illegitimate genotypic and phenotypic features of FL (developmentally blocked GC B cells and imprints of AID-mediated genomic instability) (14, 16). High t(14;18) frequencies were also fortuitously detected in prediagnostic blood samples from healthy individuals who subsequently developed FL up to 20 years later (17, 18) and in samples from allogeneic donors who developed FL synchronously with the BM recipients (19, 20). The long latency observed in these cases, combined with the persistence of t(14;18) clones over more than 10 years of follow-up (21), provide further evidence that FL is preceded by an insidious preclinical phase of asymptomatic growth and might emerge from precursor clones evolving over years, if not decades.

The mechanisms governing the transition and progression from t(14;18)+ B cells to early FL precursors are to date unknown. Here, we sought to address this important issue by tracking early FL precursor dynamics throughout human and mouse B cell ontogeny.

Results

A mouse model mimicking t(14;18) translocation in healthy humans. To recapitulate the primary events leading to the generation of FLLCs and FLIS cells, we engineered a mosaic mouse model (*BCL2*tracer), in which sporadic and conditional *BCL2* transgene activation aims to mimic the rare occurrence of t(14;18) in the BM. The *BCL2*tracer mouse, in which the expression of a functional human *BCL2* (hu*BCL2*) transgene is contingent on its inversion by V(D)J recombination, recreates the sporadic occurrence of the t(14;18) translocation event in humans (~10^{-6}), induced at the appropriate developmental stage (BM pro–/pre–B cells), and generates a unique coding joint (referred to herein as *BCL2*CJ) substituting the human t(14;18) translocation between BCL2 and the Ig heavy chain junction region (BCL2/J$_H$) as a clonotypic marker (Figure 1A and Supplemental Figure 1; supplemental material available online with this article; doi:10.1172/JCI72415DS1). In this sporadic model, the preservation of normal B cell populations (Supplemental Figure 2) allows the evaluation of selective modifications of the initial *BCL2*CJ frequency following perturbations

(such as immunization) and tracking of the clonal evolution of BCL2+ cells in otherwise healthy mice.

We first used sensitive fluctuation PCR (F-PCR) assays (primers 1 + 2) to monitor BCL2 expression over time in resting *BCL2*tracer mice (Figure 1, B and C). Similar to t(14;18) in healthy humans, we observed variable low *BCL2*CJ frequencies (from <10^{-6} to 5×10^{-5}) in blood and lymphoid organs (but not in liver or kidneys). As expected in resting conditions, *BCL2*CJ frequencies monitored on sorted B cell fractions showed that most huBCL2+ cells were naive B cells (Figure 1D, white bars). Accordingly, staining for peanut agglutinin (PNA) and huBCL2 on histological spleen sections showed limited GC formation and did not reveal the presence of spontaneous BCL2+ FLIS-like structures, even in aged mice (Figure 1E, top panels).

We then tested the central FL hypothesis that rescue from apoptosis of activated GC B cells with enforced BCL2 expression provokes their accumulation in situ and maturation block. To drive naive B cells into the GC reaction, we performed short-term immunization (Figure 1F) using sheep red blood cells (srbc), which are known to induce a large polyclonal response in mice. Alternatively, *BCL2*tracer mice were bred with *Lat*Y136F mice, in which uncontrolled Th cell signaling provokes massive GC entry and activation of naive B cells in an antigen-independent manner (22). Upon such activation conditions, GC and post–GC B cell subsets became apparent on IHC (Figure 1E, bottom panels) or FACS (Supplemental Figure 2). Confocal microscopic analysis showed rare frequencies of transgenic huBCL2 protein expression (Figure 1F). However, we observed no huBCL2+ FLIS-like clusters by IHC (Figure 1E, bottom panels) or confocal microscopy (Figure 1F). We thus performed F-PCR to evaluate the relative frequency of BCL2+ cells (*BCL2*CJ) in each of the purified B cell fractions following immunization (Figure 1D, middle panel) or breeding with *Lat*Y136F mice (Figure 1D, right panel). We observed no significant increase in *BCL2*CJ frequencies in the GC fractions compared with that in memory or terminally differentiated plasma cells (Figure 1D). We conclude that during the first GC transits, BCL2+ GC B cells do not accumulate in situ, but rather differentiate into plasma or memory cells. This strongly argues against a model in which BCL2, by driving rescue from apoptosis, would provoke early differentiation arrest and GC accumulation of t(14;18)+ GC B cells and eventual FLIS formation.

Chronic immunization drives preferential accumulation and reentry of activated BCL2+ B cells into the GC. If most t(14;18)+ cells transiting for the first time through the "founder GC" initially exit as genuine terminally differentiated memory B cells, how do these cells progress back to FL precursors and FL? In line with an increasing t(14;18) incidence with age and the late onset of FL, Bende et al. have proposed that lymphoma progression does not arise during the first GC passage, but may gradually develop in memory B cells during successive/episodic recall responses throughout life (5).

We thus tested whether long-term antigenic stimulation preferentially stimulated the proliferation of BCL2+ B cells by tracking the evolution of their frequency during chronic immunization in BCL2tracer mice (Figure 2A). To do so, we used the *Aid-Cre Rosa-EYFP* mice (in which EYFP is expressed in activated B cells upon AID expression during their first passage in the GCs; ref. 23). BM progenitors from these mice were transduced with a retrovi-
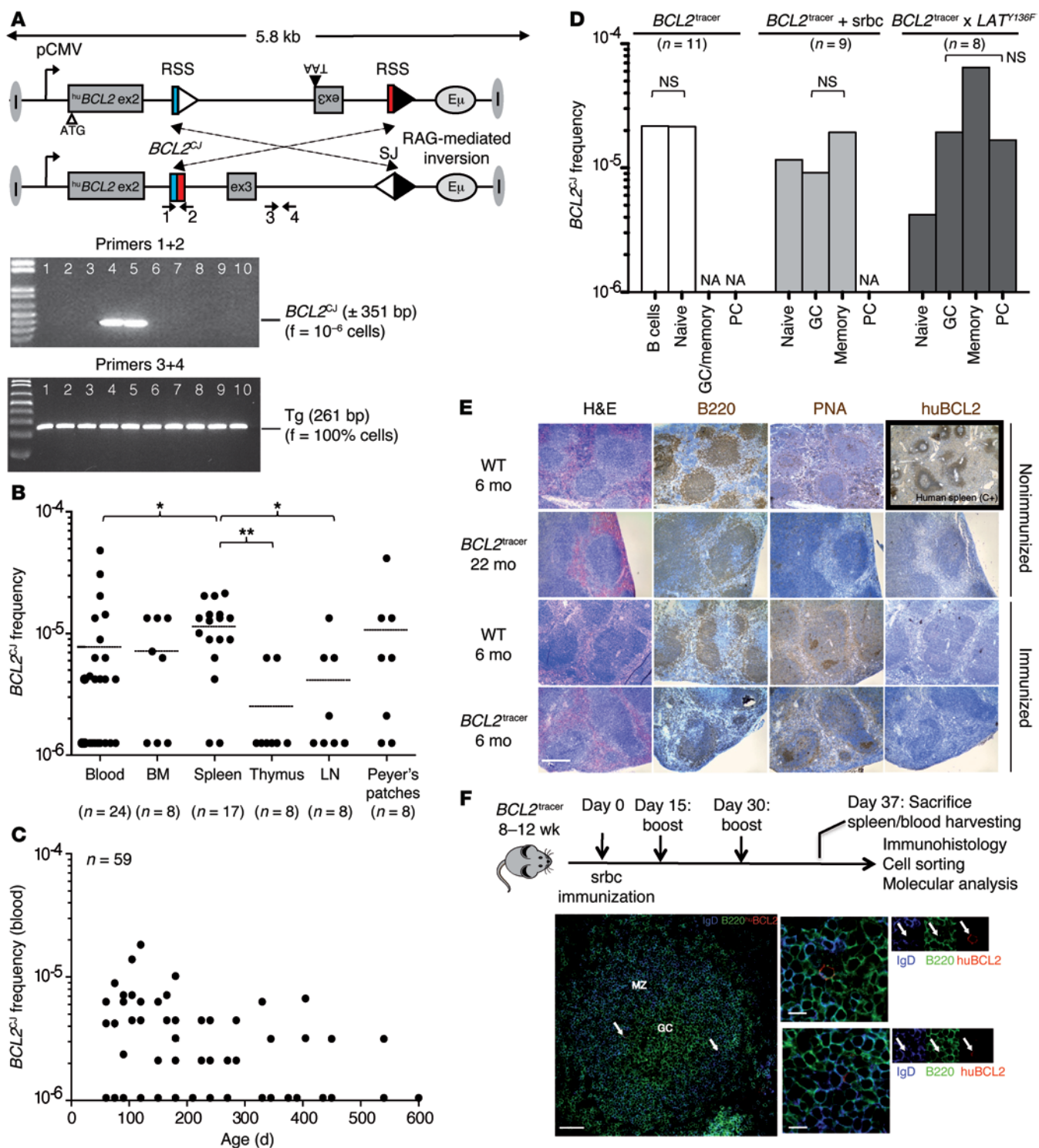
Figure 1. The sporadic *BCL2*^tracer model. (**A**) Germline and rearranged configuration of the *BCL2*^tracer transgene by RAG-mediated inversion. Only the rearranged configuration allows the expression of a full-sized, functional huBCL2 oncoprotein. Recombination signal sequences (D_H3-RSS, J_H6RSS) are indicated by triangles. V(D)J-mediated coding joints (*BCL2*^CJ) and signal joints are indicated. A representative F-PCR screen from a 3-month-old mouse shows the presence of the transgene in all replicates (3+4, bottom) and a sporadic clonotypic *BCL2*^CJ rearrangement in a few replicates (1+2, top). The frequency of inversion is calculated using Poisson's assumption based on the number of positive PCRs and input DNA. ex, exon; f, frequency. (**B**) *BCL2*^CJ frequency evaluated by F-PCR in lymphoid organs and blood from 2- to 12-month-old *BCL2*^tracer mice. Black lines represent the mean. *$P < 0.05$; **$P < 0.01$. (**C**) *BCL2*^CJ follow-up with aging in blood at steady state. (**D**) *BCL2*^CJ frequency in total spleen and cell-sorted B cell subpopulations from resting (white bars) and challenged mice (light and dark gray bars). Pooled splenocytes (3–5 mice) were used in each condition. NA, absent or too small to sort. (**E**) IHC of unchallenged or srbc-immunized *BCL2*^tracer mice stained with B220 (pan-B), PNA (GC marker), and huBCL2 antibodies. A human spleen was used as a positive control for huBCL2 staining. PNA was used instead of GL7 (44) because of better staining intensity. Scale bar: 500 μm. (**F**) Immunization scheme and immunofluorescence (IF) microscopy of *BCL2*^tracer spleen sections stained with IgD (blue), B220 (green), and huBCL2 (red) antibodies. IgD staining indicates GC boundaries. Arrows point to rare huBCL2^+ cells. Scale bars: 100 μm (left panel), 20 μm (middle panels).
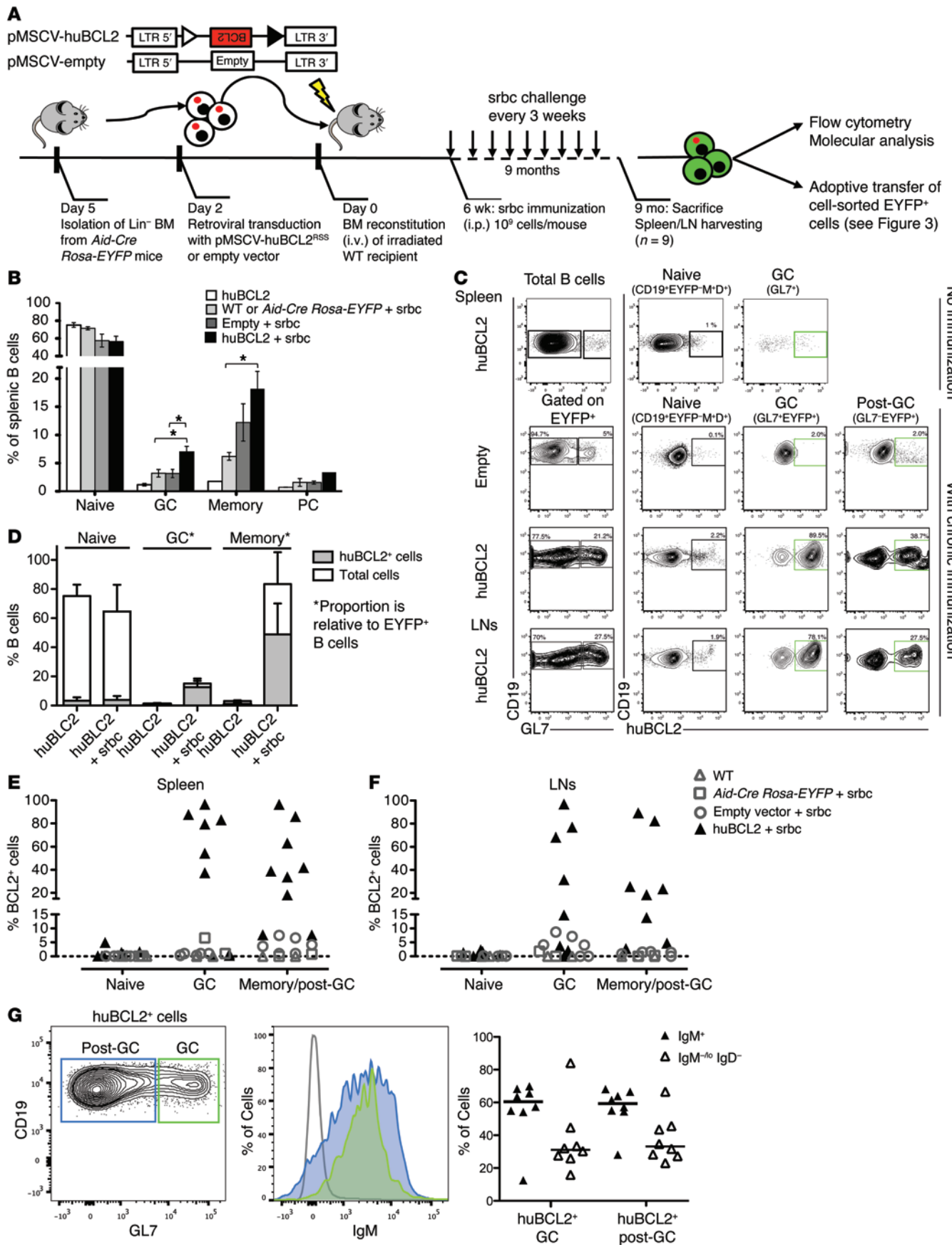
Figure 2. Chronic immunization drives preferential accumulation and reentry of activated BCL2+ B cells in the GC. (A) Schematic of BMT and chronic immunization assays; hematopoietic stem cells were transduced with an inactive (unrearranged) huBCL2, a small fraction of which (~10^{-5}) will rearrange (and thus express huBCL2) during pro–B cell differentiation. **(B)** Distribution of the splenic B cell subsets by flow cytometric analysis from unchallenged versus chronically immunized hu*BCL2*-transduced and control animals. Spleens were collected after 6 and 9 months, respectively. Values are shown as the means ± SEM from 3 independent experiments with 2 to 4 mice per group. *$P < 0.05$ and **$P < 0.01$ by Student's t test. **(C)** Representative flow cytometric profiles of splenocytes and peripheral LNs (inguinal, brachial, and mesenteric) from control (empty vector) and hu*BCL2*-transduced mice with or without chronic immunization. **(D)** Relative proportion of huBCL2+ cells in the indicated splenic B cell subsets from unchallenged versus chronically immunized hu*BCL2*-transduced animals. Note that in the absence of immunization, the percentage of EYPF+ cells was less than 1%. **(E** and **F)** Frequency of huBCL2+ cells identified by FACS as in **C** are plotted for the whole cohort of chronically immunized mice. Spleen (left panel) and LNs (right panel). Values from individual mice are shown, summarizing 3 retroviral transduction experiments, with 2 to 4 mice per group, except for WT and *Aid-Cre Rosa-EYFP* mice (1 mouse/experiment). **(G)** FACS analysis showing surface IgM expression in BCL2+ GC and post-GC B cells from *BCL2*-transduced mice.

rus-based *BCL2*[tracer] construct, keeping the sporadic occurrence of *BCL2* inversion (driven by recombination-activating genes [RAGs] in the BM). To mimic chronic antigenic recall, we immunized chimeras with srbc every 20 days for 9 months (starting on day 45). Upon sacrifice, no significant splenomegaly was manifest. Nevertheless, chronically immunized hu*BCL2*-transduced mice showed a significant increase in GC and memory B cells compared with that seen in controls (WT/empty vector) (Figure 2B). We then measured the distribution of huBCL2+ cells among the total population of EYFP+ activated B cells. Strikingly, we observed a massive accumulation of huBCL2+ cells in GC and memory B cell compartments (up to 90%), but not in naive B cells (Figure 2, C–F) or in unstimulated conditions (Figure 2D). Importantly, in both compartments, BCL2+ cells remained predominantly IgM+ (60% of cells) (Figure 2G). This indicates that upon repeated antigenic challenges, constitutive BCL2 expression in GC and memory B cells confers a considerable selective advantage over their BCL2– counterparts, in line with an enhanced GC reentry. Notably, this subtle widespread expansion and GC colonization by huBCL2+ B cells in the absence of macroscopic tissue distortion is in line with the early, nonmalignant phases of indolent lymphomagenesis in human FLIS, which can progress to overt disease with low frequencies (~5%) and long latencies (several years or decades) (12).

To formally assess whether these huBCL2+ B cell expansions occurred through cycles of GC exit and reentry and repeated rounds of GC reaction, we took advantage of EYFP labeling. EYFP+ splenic GC or post-GC B cells from 4 chronically immunized mice were cell sorted and adoptively transferred (~20,000–50,000 cells/transfer) into WT mice (preimmunized and reboosted once with srbc) (Figure 3A). Mice were sacrificed 1 week later, and *BCL2*[CJ] was monitored in total and cell-sorted spleens. Remarkably, despite the very low quantity of transferred cells and the short time allowed after transfer, *BCL2*[CJ] could be observed in the spleen (Figure 3B) and was enriched in activated B cell fractions from recipient mice (Figure 3C). We found identical clones in recipient mice that received the GC or post-GC fraction, showing

the dynamics of GC and post-GC clones in the donor mice (Figure 3B and Supplemental Table 1). huBCL2+GL7+ B cells could also be observed by confocal analysis in the GCs from recipient mice adoptively transferred with GL7+ (Supplemental Figure 3A) and GL7– post-GC fractions (Figure 3D), demonstrating that differentiated post-GC huBCL2+ memory B cells can rapidly return to the GC upon antigenic recall. To further study the role of IgM expression in the reentry process, we independently transferred GL7+IgM+ and GL7+IgG+ fractions purified from *BCL2*[tracer]-transduced mice. Interestingly, huBCL2+IgG+ B cells showed mostly an extrafollicular localization in the red pulp of the spleen, suggesting that they did not return to the GCs after stimulation, or at least not to the same extent as did huBCL2+IgM+ cells (Supplemental Figure 3B). The return to the GC of BCL2+ cells thus appears to be highly dependent on the expression of IgM on the cell surface.

Is this GC reentry able to drive a new round of GC reactions? In a series of consecutive sections from recipient mice, we observed the tight clustering of huBCL2+ B cells in a single GC surrounded by negative ones (Figure 3E and Supplemental Figure 3, A and B). This suggested the entry of a single huBCL2+ B cell, followed by in situ clonal proliferation, histologically mimicking a human FLIS cell (Figure 3E). Total cells from 1 section were scraped off the slide, DNA extracted, and *BCL2*[CJ+] monitored. We observed a drastic increase in *BCL2*[CJ] frequencies and a reduction of clonality (1 dominant clone was amplified in 100% of the F-PCR lanes; Figure 3F and Supplemental Table 1), in line with the clonal features of FLIS. Notably, this clone was also dominant in the other recipient mouse from the same donor (Figure 3B), suggesting that it acquired enhanced capabilities to colonize GCs and reactivate GC reactions. VH gene analysis confirmed the emergence of progressive clonal restriction in some GCs before adoptive transfer, along with the occurrence of intraclonal variation (ICV) due to ongoing AID activity (Supplemental Table 2).

Recent genomic studies have shown that human FLIS samples have already acquired additional alterations in addition to t(14;18) (24, 25). We thus investigated whether the enhanced capacity of BCL2+ cells to undergo iterative GC reactions in chronically challenged *BCL2*[tracer] mice is accompanied by an accumulation of genomic instability and potentially mimics genetic features of human early FL entities. We performed exome sequencing on purified BCL2-enriched GC and memory cell fractions from 3 chronically immunized (*BCL2*-transduced) mice and 1 control (empty vector) mouse (Supplemental Table 3). BCL2-low (≤1%) naive fractions from the corresponding mice were also sequenced and used as a germline reference. Due to the low DNA content per subset, we performed whole-genome amplification (WGA) before sequencing. The 50-Mb exome capture was sequenced to a mean depth of 172X across all mice (range = 118X–214X; Supplemental Table 3). We used a stringent bioinformatic filtering pipeline to remove known genetic and recurrent false-positive variants (Supplemental Figure 4). Overall, from an initial set of several thousands of raw variant calls, the cumulative filtering of and focusing on protein-altering changes identified between 111 and 2,565 nonsilent (nonsynonymous, stop gain, or stop loss) single nucleotide variants (SNVs) per B cell subset in the *BCL2*-transduced mice compared with 63 to 70 SNVs in the control mouse (Figure 4A and Supplemental Table 4). In all *BCL2*[tracer]-transduced mice, the
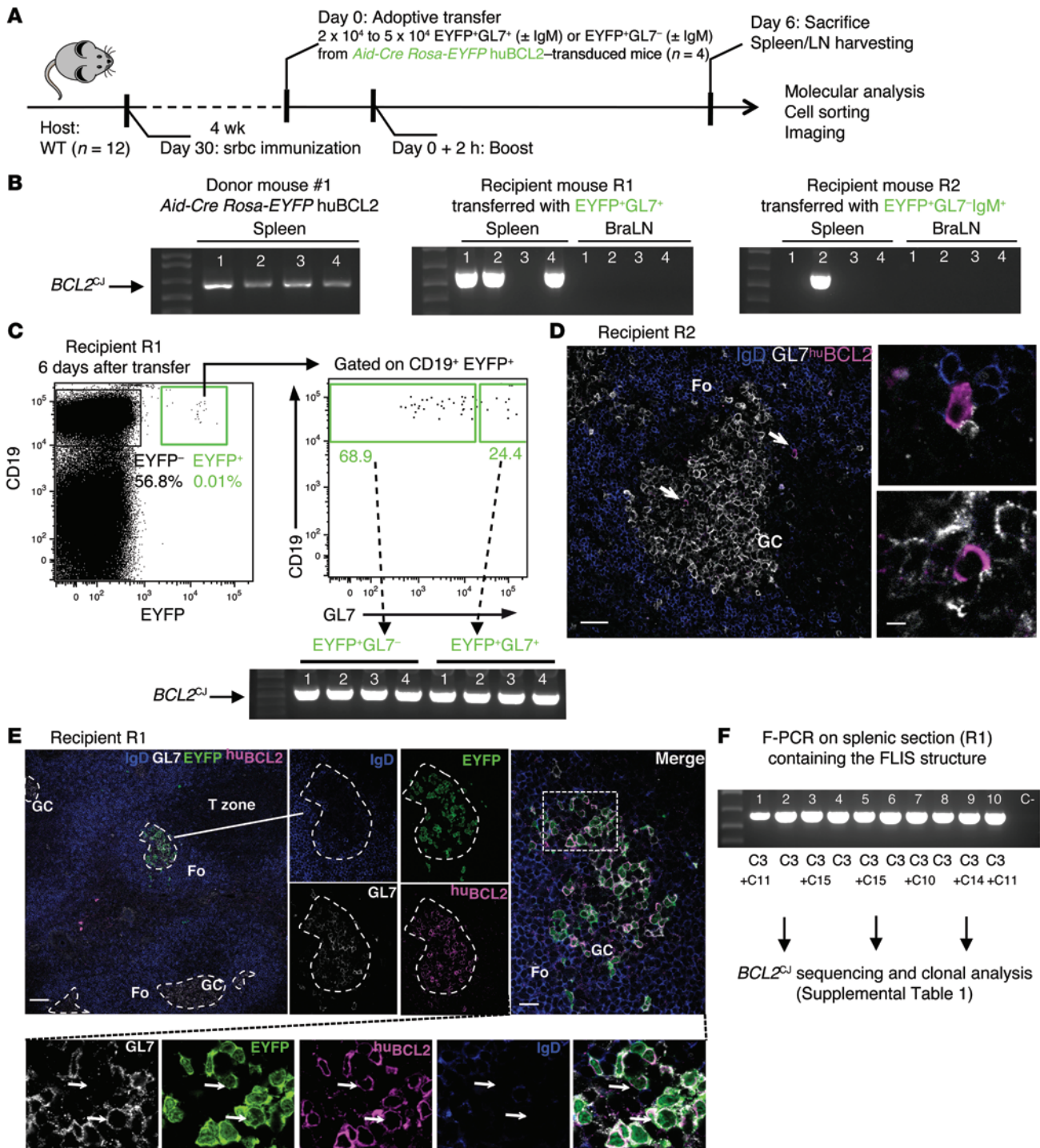
Figure 3. BCL2+ GC and post-GC B cells are able to reenter and reactivate GC reactions during repeated antigenic challenges. (A) Schematic of the adoptive transfer procedure. **(B)** Representative F-PCR analysis of *BCL2*^{CJ} junctions in total spleen and LNs harvested before (left panel) and after adoptive transfer of the indicated EYFP+ cell subpopulations (middle and right panel). BraLN, brachial LN. **(C)** FACS plots showing the retrieved EYPF+ cells in recipient mouse R1 6 days after adoptive transfer of EYFP+GL7+ cells and F-PCR analysis of *BCL2*^{CJ} in FACS-sorted EYFP+GL7+ and EYFP+GL7– cells. 650 EYFP+GL7– and 250 EYFP+GL7+ cells were recovered from the EYFP+ cell subpopulation (0.01% of total splenic B cells). **(D)** Spleen histology from recipient mouse R2 after adoptive transfer of EYFP+GL7–IgM+ cells, stained with IgD (blue), GL7 (white), and huBCL2 (pink) antibodies. huBCL2+ cells in GCs and peri-GCs are shown (arrows). Images are representative of 2 independent experiments with 2 mice per condition. Scale bars: 50 μm (left) and 10 μm (right). **(E)** Splenic histology from recipient mouse R1 after adoptive transfer of EYFP+GL7+ cells. A single GC invaded with huBCL2+EYFP+ cells was observed among otherwise normal GCs (dashed line outlines), mimicking a human FLIS. Arrows indicate the presence of both GL7+ and GL7– BCL2+EYFP+IgD– cells in the same GC. Images are representative of 3 independent experiments with 2 mice per condition (additional figures in Supplemental Figure 3, A and B). Fo, follicular zone. **(F)** F-PCR of *BCL2*^{CJ} in the splenic section containing the FLIS structure that was scraped off the slide. Ten PCR replicates of 100 ng DNA each were performed in parallel, cloned, and sequenced. Scale bars: 200 μm (left) and 30 μm (right).
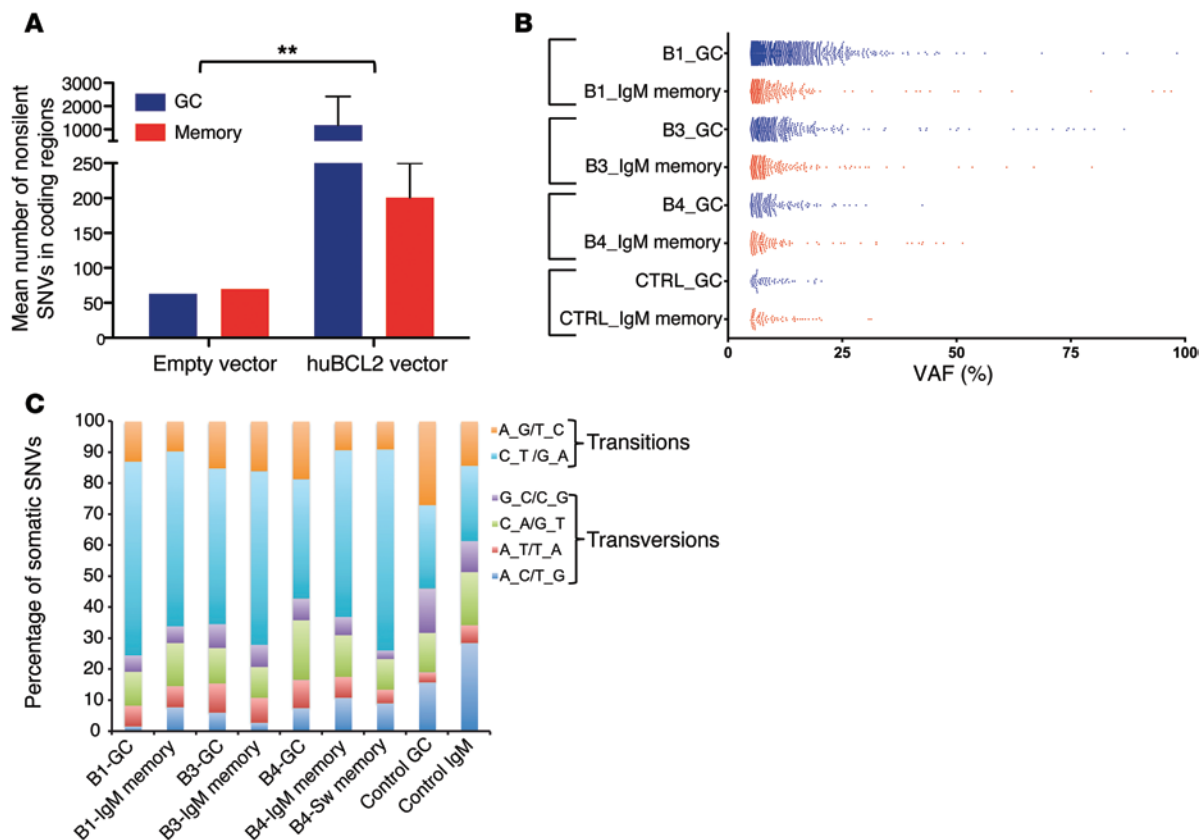
Figure 4. Somatic mutation analysis of BCL2-enriched GC and post-GC subsets by exome sequencing. (**A**) Histograms of the mean number (± SEM) of non-silent SNVs in BCL2-enriched GC and post-GC subsets from BCL2 and control mice. (**B**) Frequency distribution of VAFs for all the gene loci variants identified in each B cell subset from *BCL2*-transduced versus control (empty vector) mice. (**C**) Base-level transitions and transversions of all variant loci shown in **B**.

GC fractions exhibited an increased frequency of SNVs relative to those in matched IgM or switched memory cell fractions. We found most of the detected SNVs at low variant allelic frequencies (VAFs) (5%–25%), while a limited set of gene mutations presented at higher frequencies (>30%) and were present in the distinct fractions of a given mouse (Figure 4B and Supplemental Table 5). Finally, G→A and C→T transitions were the most common nucleotide substitutions, consistent with AID-mediated activity (Figure 4C). Altogether, this suggests that huBCL2+ B cells accumulating in GCs upon chronic immunizations collected additional mutations at a significantly higher rate than did their BCL2– and peripheral counterparts (normal GC and memory B cells). Importantly, the large number of mutations at low VAFs parallels the situation in human FLIS, in which recurrent FL hits are rarely observed (24, 25). In both cases, human FLIS and murine FLIS-like cells thus seemingly stand at a crossroads between increased genomic instability and low selective pressure for malignant transformation (24), consistent with their low rate of progression to overt FL (12).

We conclude that chronic immunization favored dissemination of BCL2+ B cells, iterative GC reentry, preferential clonal expansion, and eventual progression into structures resembling human FLIS, the earliest known precursor of FL development.

FL-like clones expand and disseminate extensively in human blood and tissues. To validate and extend our observations in humans, we reasoned that the more t(14;18)+ cells undergo rounds of GC exit and reentry during a lifetime, the more they should expand, dis-

seminate to various distant lymphoid organs, independently accumulate imprints of AID activity (somatic hypermutation [SHM] and class switch recombination [CSR]), and clonally diverge during clonal expansion.

The extent of dissemination was first examined in paired lymphoid tissue samples (spleen, LN, BM) and blood from a large cohort of healthy organ donors, defined here as individuals devoid of manifest hematological conditions (Supplemental Table 6). We performed semiquantitative F-PCR to evaluate the presence of t(14;18) and estimate t(14;18)+ cell frequencies in paired blood and lymphoid tissue. This assay allowed us to detect BCL2/J_H translocation with a sensitivity of 1 positive cell per 500,000 normal lymphocytes. Remarkably, this analysis revealed that a large fraction of the t(14;18)+ cell pool is actually homing to tissues (Figure 5A). We found that t(14;18)+ B cells displayed a wide range of cell frequencies in most adult lymphoid tissues from most individuals (Figure 5B), including in the BM, where positivity correlated well with blood (Figure 5C), as previously observed in FL (18, 26). BCL2/J_H breakpoint analysis (Supplemental Table 7, A–C) showed that t(14;18) cell frequencies systematically resulted from the expansion of 1 dominant clone (Figure 6A), disseminated in most paired tissues analyzed, with good correspondence of clonal distribution between blood and tissues (Figure 6B).

Molecular analysis of Sμ/Sγ regions on the translocated alleles of resident t(14;18)+ B cells showed the occurrence of SHM and/or CSR in more than 98% of cases, consistent with their status as
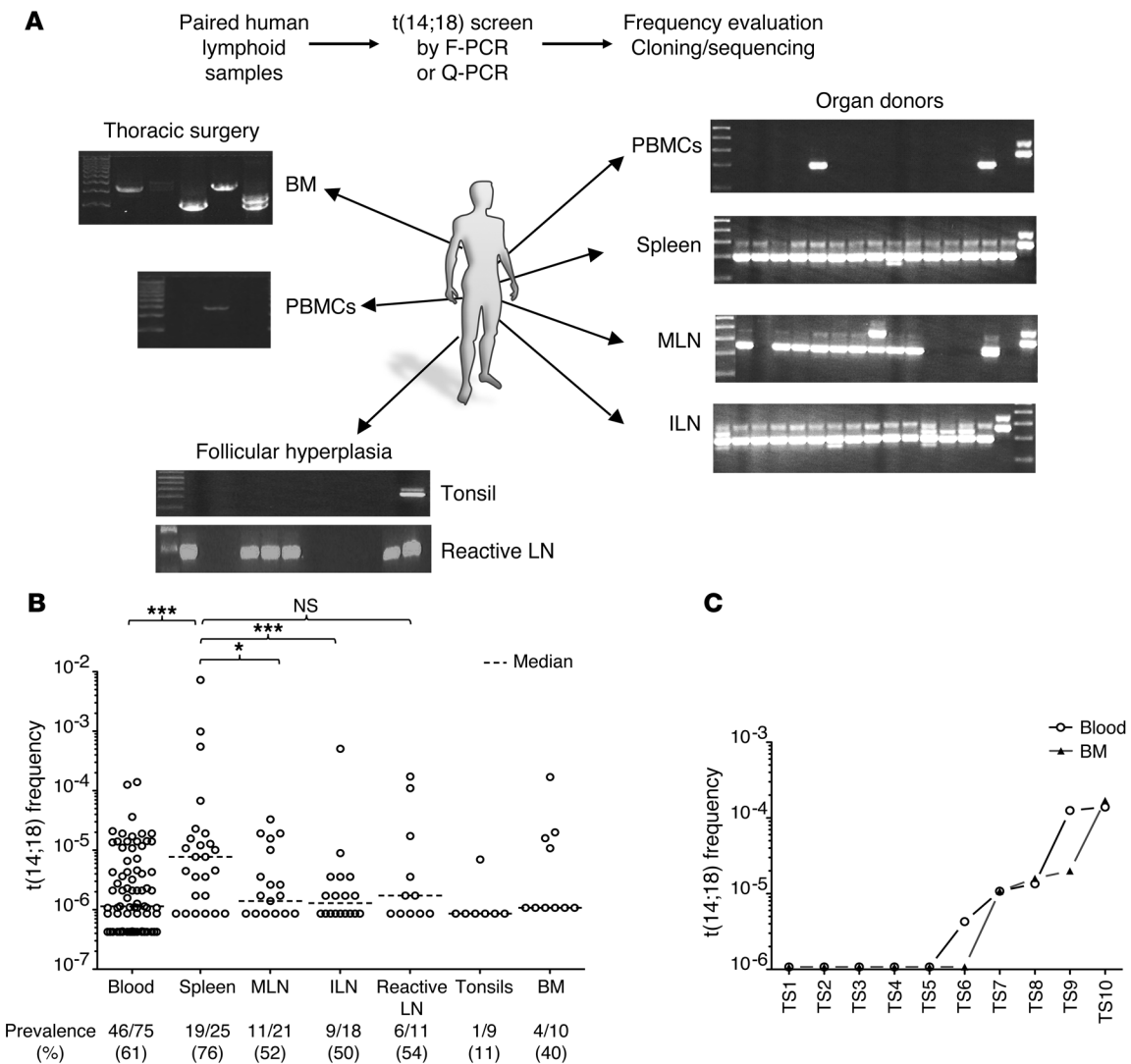
Figure 5. t(14;18)+ cells are present in blood, BM, and lymphoid organs from healthy individuals. (**A**) Representative F-PCR screen of t(14;18)+ cells in paired lymphoid tissue samples from organ donors. F-PCR and quantitative-PCR (Q-PCR) analysis allowed determination of both t(14;18) frequency and clonality (through BCL2/J$_H$ breakpoint sequencing). (**B**) Prevalence and frequency of t(14;18)+ cells in lymphoid organs and blood (compiled from Supplemental Table 7); additional blood samples were obtained from a blood bank. The detection threshold was approximately 10^{-6}. (**C**) Prevalence and frequency of t(14;18)+ cells in paired BM and blood samples from thoracic surgeries. ILN, iliac LN; MLN, mesenteric LN; PBMCs, peripheral blood mononuclear cells. *$P < 0.05$, ***$P < 0.005$.

GC-derived B cells (Supplemental Table 8). Accordingly, t(14;18) was rarely detected in the sorted naive B cell subset (Figure 6C and Supplemental Table 9). Within the memory B cell subset, t(14;18) was predominantly observed in the IgD/M memory B cell fraction. This "allelic paradox" (expression of surface IgD/M in a cell with a switched translocated allele) is unusual in normal memory B cells but stands as a hallmark of FL and circulating FLLCs, presumably as the result of strong selection pressure to signal through IgM (9). We next used discriminant markers to visualize and further characterize these cells by confocal analysis using BCL2 and BCL6 expression, which is normally mutually exclusive in B cells (27). In FL and FLIS, however, t(14;18)+ cells are frozen "GC-like" B cells and present atypical BCL2+/BCL6+/lo double staining inside and outside the GCs. Using a BCL2/BCL6/CD3/CD19 multicolor IF staining combination, we could observe sporadic CD3^{neg} BCL2+/BCL6+/CD19+ triple-positive cells inside and outside the GCs

in nonreactive spleen from organ donors (Figure 7, A and B, and Supplemental Figure 5), with good correlation with molecular frequencies (Figure 7C).

Altogether, this suggests that t(14;18)+ clones homing to tissues are an atypical "GC-like" clonal B cell population that extensively disseminated in "healthy" individuals, long before malignant transformation.

The subversion of t(14;18)+ memory B cell dynamics drives sustained AID mutator activity. We next monitored clonal divergence. A clone is made of many single daughter cells (subclones) that are potentially disseminated in remote tissues. In the presence of AID, SHM and CSR independently accumulate in each subclone, and this ICV can be used to track their genealogical history during clonal expansion (Figure 8A). If the global pool of t(14;18)+ cells results from protracted GC coopting over many years, subclones should display more ICV than do normal memory B cells in the
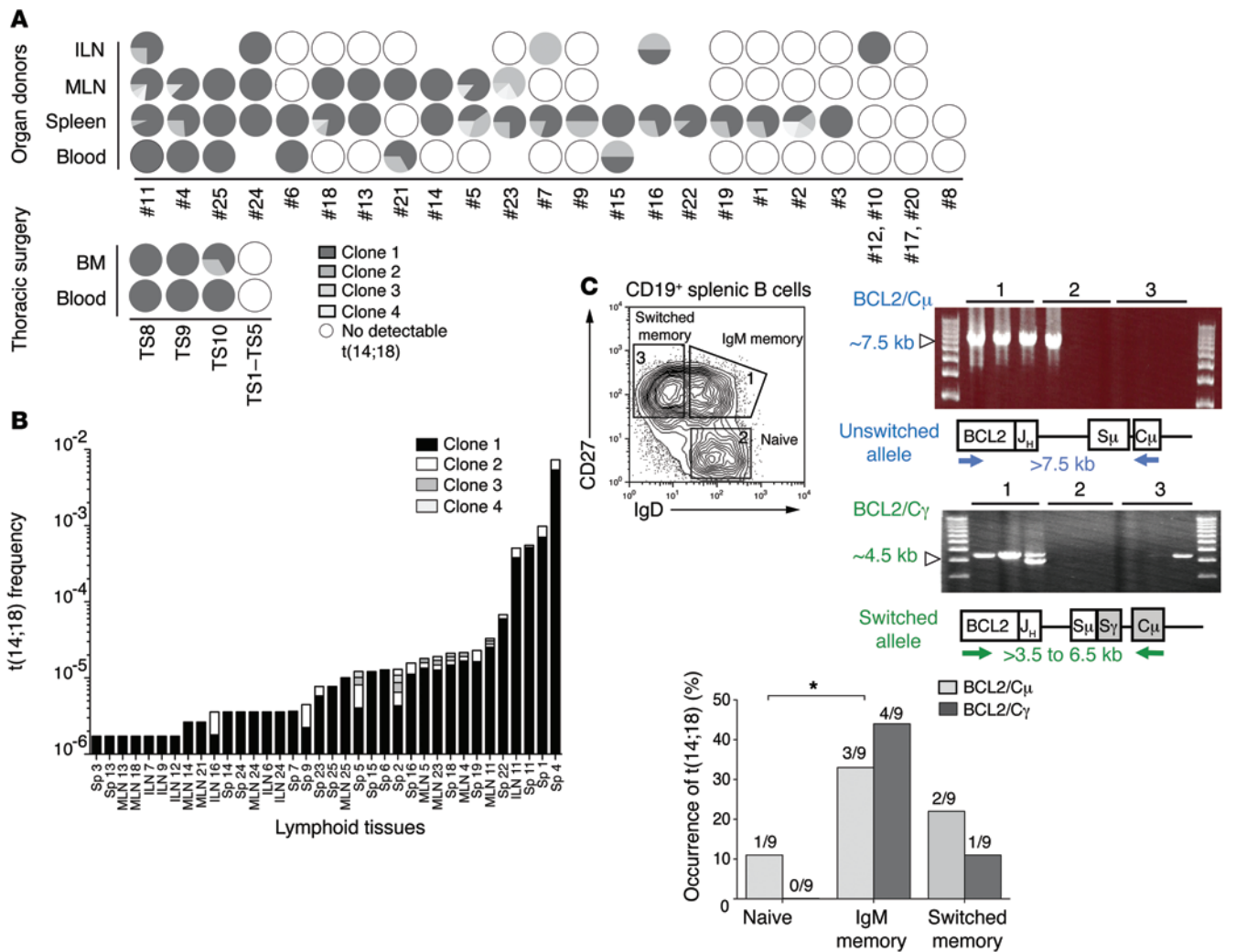
Figure 6. Molecular characterization of resident t(14;18)+ cells in lymphoid organs from healthy donors. (**A**) Relative clonal distribution in paired samples (compiled from Supplemental Table 7). Each clone [defined as t(14;18) from the indicated donor displaying the same BCL2/J_H breakpoint] is coded by gray shading within the circles. White circles indicate t(14;18)− samples; absence of a circle indicates that the tissue was not available. (**B**) Clonal expansion in organ donor's samples. Clones from above are coded by gray shading according to their relative frequency in the indicated tissue and individual. Sp, spleen. (**C**) Geno-phenotypic characterization of resident t(14;18)+ clones. Top panel (left): Cell-sorting strategy of splenic B cell subsets (according to CD19, CD27, IgD, and IgM expression). Top panel (right): Representative long-range F-PCR on indicated B cell subsets. BCL2/Sμ amplifies unswitched translocated alleles; BCL2/Sγ amplified switched translocated alleles. Bottom panel: Overall distribution of switched versus unswitched t(14;18) alleles in the B cell subsets from 3 human samples (see Supplemental Table 9 for raw data). Cμ, constant mu region; Cγ, constant γ region; Sμ, switch mu region; Sγ, switch γ region.

same individual. To test this hypothesis, we tracked t(14;18)+ subclones as single cells in paired distant tissues (spleen, LNs, or BM) and blood using fluctuation long-range PCR (F-LRPCR). LRPCR (~3–7 kb; Supplemental Figure 6A) was required to encompass on the same amplicon both the BCL2/J_H junction (the clonotypic root) and the Sμ/Sγ intronic region in which CSR and SHM accumulate (28). Genealogical trees were then built using the BCL2/J_H junction as the tree root and SHM- and CSR-based ICV to branch the subclones. Remarkably, out of 6 genealogical trees generated from 45 sequenced amplicons, we found all subclones to be distinct (Figure 8B). Furthermore, the distant branching of clonal variants disseminated in remote organs (e.g., donor 11) and the fairly large number of mutations between the closest neighbors (especially when belonging to distinct compartments) indicated that many more intermediate subclones and branching are miss-

ing from the trees than is apparent. The considerable clonal divergence of branched subclones largely disseminated in distant tissues concurs with a dynamic model in which iterative rounds of GC reactions occur over prolonged periods. Interestingly, we also observed such clonal divergence in t(14;18)+ subclones from the paired LN and blood samples of an FLIS case, suggesting similar molecular dynamics for both precursor entities.

To comparatively track the dynamics of normal memory B cells, we attempted a similar F-LRPCR strategy, substituting the *BCL2* primers with V_H primers (V_H6 family, V_H3-23) (Supplemental Figure 6B). However, and in contrast to BCL2/Sμ/Sγ, we repeatedly failed to amplify the VH/Sγ clones twice in the spleen, indicating a substantially lower clonal expansion of normal versus t(14;18)+ memory B cell clones. To still gain comparative information on the dynamics of normal memory B cells, we increased
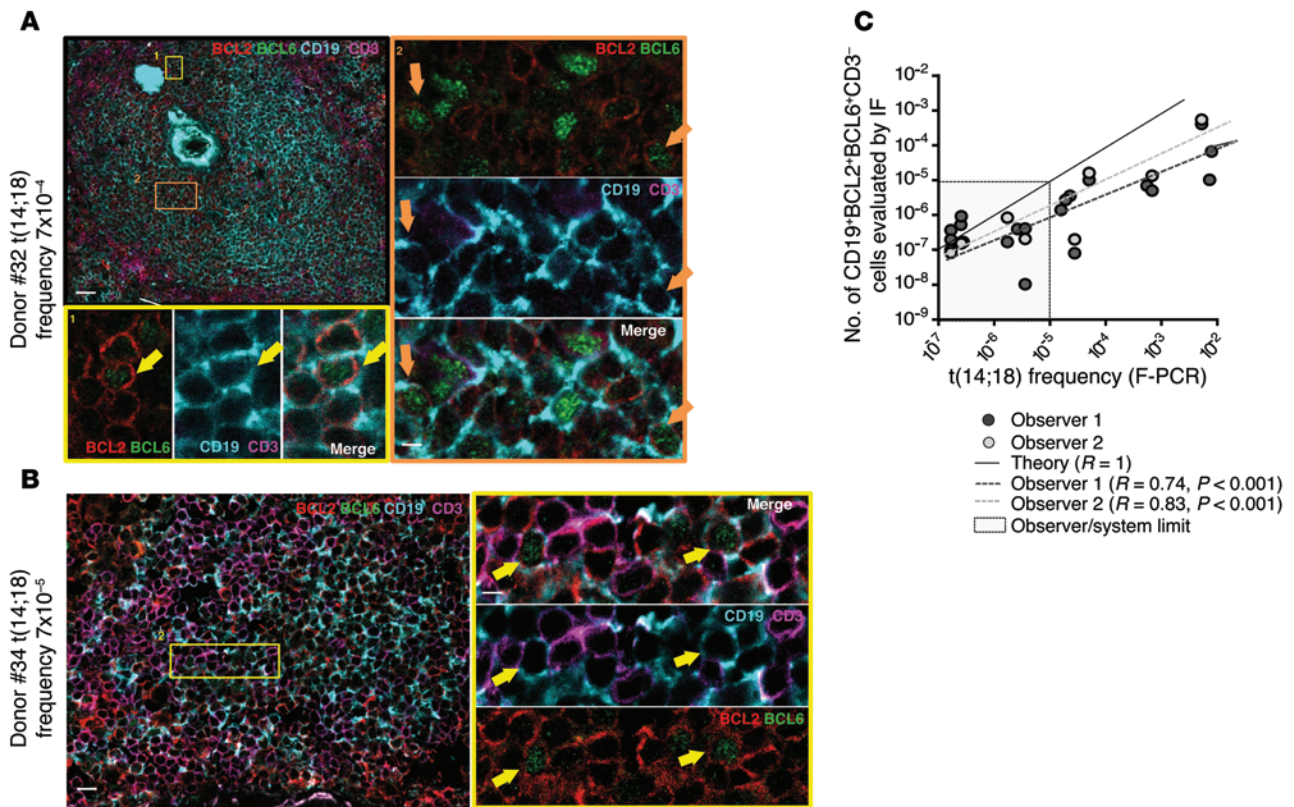
Figure 7. Resident t(14;18)⁺ cells coexpressing BCL2 and BCL6 in organ donors' secondary lymphoid organs. (**A** and **B**) Representative IF staining of 2 organ donors' t(14;18)⁺ spleens. CD3ⁿᵉᵍ BCL2⁺/BCL6⁺/CD19⁺ cells are indicated with yellow arrows. (**C**) Correlation plot showing the frequency of CD3ⁿᵉᵍ BCL2⁺/BCL6⁺/CD19⁺ triple-positive cells evaluated by IF against the frequency of t(14;18)⁺ cells evaluated by F-PCR. The theoretical value ($R = 1$) is shown. Two independent observers performed the IF measurements. Scale bars: 50 μm (**A**, left) and 5 μm (**A**, right); 30 μm (**B**, left) and 5 μm (**B**, right).

amplification efficiency by reducing the size of the amplicon (29). We identified complementarity-determining region 3 (CDR3) junctions in sorted splenic memory B cell fractions and backtracked single B cell clones using a CDR3-specific reverse primer (Supplemental Figure 6B and Supplemental Table 10). Although frequencies of backtracked clones constantly remained in the low range of ~10^{-5} [while up to 1,000 times more t(14;18)⁺ clones could be found in the same organs of the same individuals] (Supplemental Table 7A), we obtained amplicons through repeated F-PCRs and built genealogical trees based on ICV in the V_H region. We seldom observed ICV, as a large amount of subclones in a given tree (up to 7) displayed strictly identical mutation patterns and/or no branching (Figure 8C), in line with a more limited history of GC coopting than that of t(14;18)⁺ clones. Accordingly, the global SHM load in the Sμ/γ region was significantly lower in normal IgM⁺CD27⁺ and switched memory B cells than in t(14;18)⁺ cells (Figure 8D).

Sustained and deregulated AID expression has been shown to be associated with lymphoma progression. A significantly higher rate of SHM and the occurrence of aberrant CSR events (Figure 8, B and E, and Supplemental Table 8) were globally observed in the Sμ/Sγ region of t(14;18)⁺ B cells compared with CD27⁺IgM⁺ and switched memory B cells. The rates and extent of SHM and CSR were particularly advanced in the paired BM and blood samples from aged individuals (up to 64 mutations, including aberrant CSR [ref. 30] and the recurrence of unusual — potentially sequential — trimming of the switch regions by ongoing CSR, similar to what

has been recently observed in repair-deficient conditions [ref. 31]; Figure 8E and Supplemental Table 8), adding to the evidence that AID-mediated events accumulate with age in persisting t(14;18)⁺ clones and niche in the BM.

We conclude that t(14;18)⁺ B cells from healthy individuals and FLIS are functionally distinct from most genuine memory B cells, with such t(14;18)⁺ B cells displaying distinctive expansion and dissemination patterns that likely result from a protracted history of GC coopting and enhanced aberrant AID activity, potentially leading to FL progression.

Discussion

It has long been inferred that reactivation of immunological memory during antigenic recall involves iterative cycles of GC reentry. Nevertheless, the formal demonstration that reactivated memory B cells indeed have the plasticity to "dedifferentiate" back into centroblasts and centrocytes and re-engage in the process of mutation and selection has been only recently achieved in mice, thereby revealing the highly open dynamics of the GC structure as well as the important functional differences between memory subtypes. A similar process seems to occur in humans, although with the caveat that this involves unknown, complex, and heterogeneous immunological histories. Using a single-cell DNA-based tracking approach, we further show here that following GC exit, human memory B cell clones disseminate not only in the blood and spleen, but also in distant lymphoid organs. Interestingly,

this raises the possibility that secondary lymphoid organs other than the spleen also constitute additional reservoirs for memory B cells (32). However, we also observed that most memory clones displayed limited clonal expansion, even in the spleen. Memory clones also showed limited clonal divergence, suggesting that in individuals with standard immunological histories (i.e., in the absence of major or chronic infectious challenge), most memory B cells are only moderately stimulated to undergo iterative cycles of GC reentry and/or GC reaction. This plasticity of memory B cells enabling their return to GC reactions can nevertheless be hijacked by t(14;18) cells, as suggested by the striking difference in both clonal expansion and clonal divergence we observed with disseminated t(14;18) clones as compared with their normal memory B cell counterparts and as directly demonstrated in the mouse upon chronic immunization and adoptive transfer of GC and post-GC BCL2+ B cells. This enhanced capability of GC reentry and reactivation likely results from several specific distinguishing properties of t(14;18) cells. First, BCL2 overexpression has been shown to extend the half-life of memory B cells (33), allowing prolonged opportunities for appropriate cognate stimulation. Second, by uncoupling differentiation from selection, BCL2 has been shown to drive the formation of a pool of BCL2+ memory B cells with loose BCR affinities (34), which might be less restrictive of cross-reactivity and/or bystander activation than are most highly selected memory B cells. Third, most t(14;18)+ and FL cells are selectively spared from switching isotypes at the expressed allele, despite active CSR and SHM, and thus express IgM — the so-called allelic paradox — that seemingly renders these cells more prone to GC reentry (9). This process would, however, require time: in the mouse, we show that prolonged or chronic immunization is necessary to incite iterative GC reentry of BCL2+ B cells, preferential clonal expansion, accumulation of genomic instability, and eventual progression into histological structures resembling human in situ FL development. In humans, it may take a lifetime to recapitulate this pretumoral phase, in line with the increased incidence of FL with age and the indolent clinical course generally observed. This further supports the evidence that FL is preceded by a similar asymptomatic preclinical phase or subclinical disease, which may last for very long periods (up to 20 years before diagnosis) (18, 35).

From an oncogenic standpoint, such frequent visits to GCs of t(14;18)+ memory B cells are great incentives for genomic instability, accumulation of genomic alterations, and lymphoma progression. The inappropriate arrest of maturation is one of the characteristic deregulated functions paving the way for transformation into cancer cells (36). This differentiation block typically occurs in FL, which classically displays a GC-like B cell phenotype (10, 37). This block seems to already be present in FLLCs (9), and we show here that these atypical t(14;18)+ cells had already colonized lymphoid organs in a large proportion of healthy individuals. How and when did recirculating t(14;18)+ memory B cells acquire this developmental arrest and progress into FLLCs? It has long been assumed that t(14;18)-driven ectopic expression of BCL2 plays a critical role in this process by allowing the rescue of centrocytes with compromised survival due to low BCR affinity. We show that mere BCL2 expression in GC B cells is actually insufficient to fix such structures. The scattered distribution of BCL2+BCL6+ B cells we observed in peri-GC and nonreactive areas of spleens and the

occasional high t(14;18) frequencies we observed in nonreactive tissues (Figure 7 and Supplemental Figure 7) suggest that resident FLLCs represent the nonreactive counterparts of FLIS, prone to (re-)colonize GCs upon appropriate immune challenge, as seen in human reactive LNs, where they accumulated in a nonproliferative GC compartment (38). Consistent with this hypothesis, we found clonal divergence between paired blood and LN subclones in a patient with an FLIS and in follow-up studies of t(14;18)+ cells persisting in healthy individuals' blood for over 10 years (21). This pretumoral pattern of clonal evolution is highly reminiscent of the evolutionary process governing FL transformation (39, 40), suggesting a common and early-acquired dynamics. In this respect, our finding of highly mutated FLLCs in the BM is of particular significance. While not a homing niche for memory B cells, the BM is a frequent invasion site in FL, and it could represent an early niche for cancer stem cells (41), in line with reported cases of synchronous FL development in donor/recipient pairs after allogeneic BM transplantation (BMT) (19, 20). Importantly, the detection of t(14;18)+ precursor FL clones in prediagnostic blood samples several years before diagnosis (17, 18, 20) supports a scenario in which some FL precursors have already acquired the defining events necessary for clonal maintenance and ineluctable malignant progression, long before symptomatic FL manifestation.

Methods

Human samples. Human samples were obtained from Hôpital de la Conception (Marseilles, France) (encephalic-death, heart-beating organ donors) and the Centre Hospitalier Universitaire (CHU) Pontchaillou (Rennes, France) (cardiac surgeries, child routine tonsillectomy, benign hyperplasia surgery) (Supplemental Table 6). FLIS samples, including one coupled to blood, were obtained from the hematopathology department of the Centre Henri Becquerel (Rouen, France) and the Institut Paoli Calmettes (Marseilles, France). All fresh samples were placed on ice immediately after surgical removal. Mononuclear cells were isolated by mincing tissues in RPMI containing 10% FCS followed by Ficoll density centrifugation.

Generation of sporadic BCL2^tracer transgenic mice. An inactive *BCL-2*^tracer transgene (5.8 kb) was cloned into the pcDNA3.1(+) vector under the control of the constitutive *CMV* promoter, flanked in 3′ by the *IGH* intronic enhancer (Eμ) and bordered by 2 chicken β-globin HS4 insulators (I) aimed to restrict the influence of the insertion sites (ref. 42 and Supplemental Figure 1A). hu*BCL2* sequences were used in order to discriminate the transgenic BCL2 protein from endogenous *Bcl2* in transgenic mice. The genomic sequences of hu*BCL2* exon 2 (containing the start codon) and exon 3 (containing the stop codon), each including part of the intronic sequences comprising the splice sites, were separately cloned in the construct in direct and inverse orientation, respectively. *BCL2* exon 3 was flanked in 3′ by an *IRES-H2BGFP* fusion gene (43), followed by a polyA sequence, both also cloned in inverse orientation. For the generation of *BCL2*^tracer transgenic mice, the choice of the D_H3/J_H6 RSS pair (RSS^lo) over the other combination (RSS^hi) was motivated by its relative low efficiency in ex vivo recombination assays (Supplemental Figure 1B), in order to mimic the low frequency of t(14;18) in humans. The functionality and oncogenic potential of the huBCL2 oncoprotein expressed from the transgenic construct was validated ex vivo (Supplemental Figure 1, C and D) and in vivo (Supplemental Figure 1E) before injection. The *BCL2*^tracer trans-
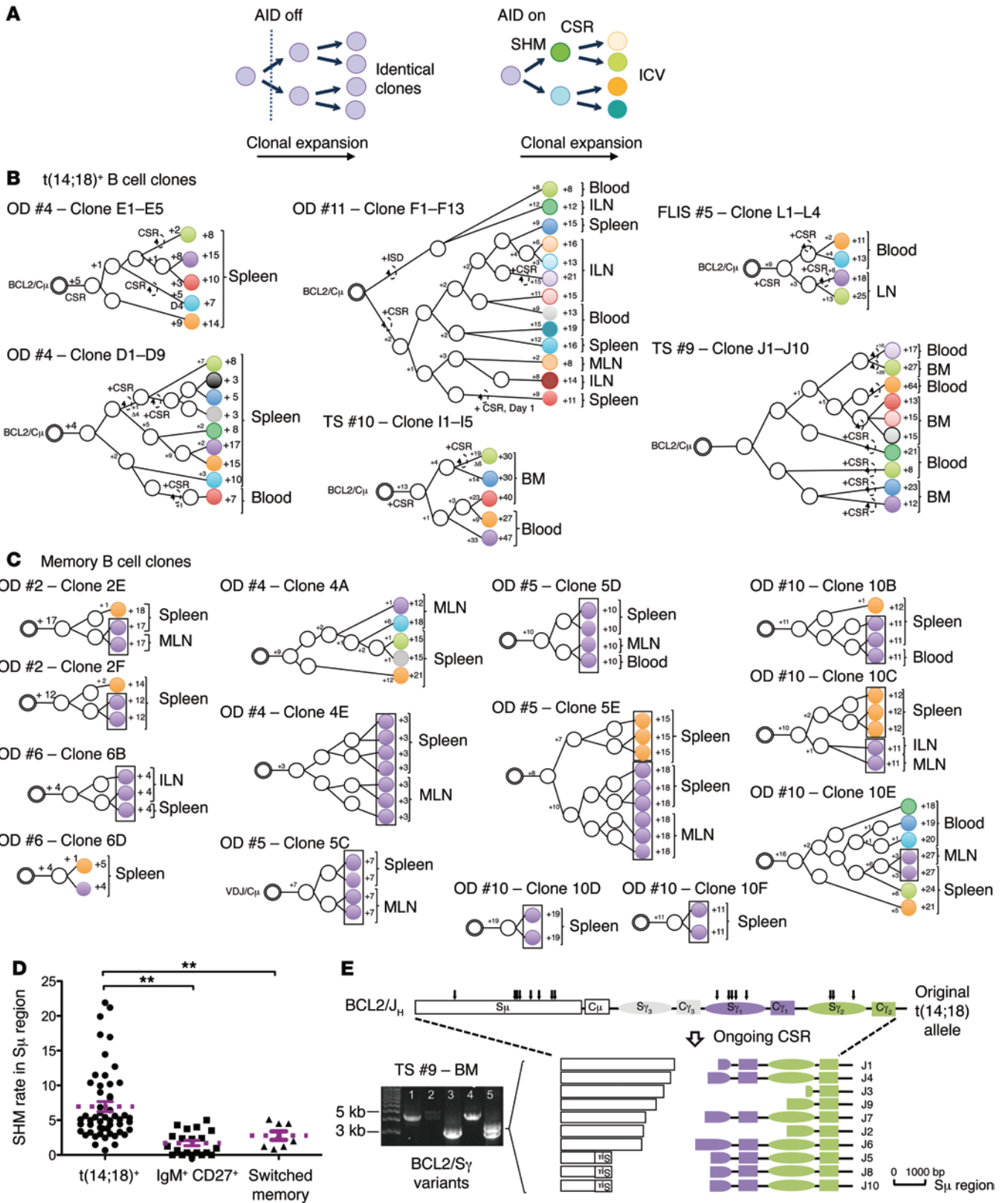
Figure 8. Clonal divergence between FLLCs and memory B cells in blood and tissues. (**A**) Schematic representation of ICV accumulating during clonal expansion in the presence of AID. Distinct subclones are designated with distinct colors. (**B**) Genealogical trees generated from t(14;18)⁺ subclones issued from 4 organ donors and 1 FLIS. Trees are rooted from an identical BCL2/J$_H$ breakpoint and organized based on ICV in the Sμ/Sγ regions of the translocated allele. Shared mutations were used to define putative intermediate filiation (white circles). Stepwise accumulation of mutations is indicated by the numbers above the branches (+1 to +64). Total mutations are summarized at the end of each branch. Dashed arrows indicate ongoing CSR. ISD, intra-switch deletion. (**C**) Genealogical trees generated from memory B cells issued from 5 organ donors. Trees are rooted from an identical V$_H$ (D)J$_H$ junction and organized based on ICV in the V$_H$ region. Identical subclones (no ICV) are boxed. (**D**) SHM rate in the switch regions from t(14;18)⁺ B cells, IgM⁺CD27⁺ B cells, and switched memory B cells. The rate is given as a percentage per 1,000 bp. (**E**) Aberrant CSR in t(14;18)⁺ variants from a paired BM/blood sample (TS #9). The amplified PCR fragments were cloned and sequenced. Arrows indicate the positions of ongoing CSR breaks and are represented below. Some clones displayed an inversion of part of the Sμ region. OD, organ donor; TS, thoracic surgery.

gene construct was microinjected into B6/CBA pronuclei, implanted into pseudopregnant females, and the littermates screened for the presence of the transgene. A *BCL2*tracer transgenic mouse line was established from a fertile male by backcrossing to a C57BL/6 background for 7 generations.

Retroviral constructs, transduction, and BMT. The *BCL2*tracer transgene in the germline (allowing sporadic expression in B cells, huBCL-2RSS) and rearranged configuration (allowing constitutive expression in all hematopoietic lineages, hu*BCL2*) was subcloned into MSCVneo retroviral vectors (Supplemental Figure 1 and Figure 2). Murine *Myc*WT and *Myc*T58A cDNAs were subcloned into an MSCV-IRES-EGFP retroviral vector (MIE). Retroviral vectors were transfected alone or cotransfected with Lipofectamine 2000 (Invitrogen) into Plat-E packaging cells. BM cells from 8- to 10-week-old C57BL/6 or *Aid-Cre Rosa-EYFP* mice were harvested, enriched in Linneg cells, and cultured overnight in RPMI containing 10% FCS, 10 ng/ml mIL-7, 10 ng/ml mFlt3-L, and 100 ng/ml mSCF (Peprotech). Retroviral supernatants were mixed with polybrene (4 μg/ml), and viruses were transduced into BM progenitors by spinoculation at 1,800 *g* for 2 hours at 33°C on 2 consecutive days, and 1×10^5 to 5×10^5 transduced BM cells were injected via the retro-orbital plexus in lethally irradiated C57BL/6 mice. All mice were monitored daily for evidence of disease, sacrificed, and autopsied upon manifest signs of disease (lethargy, organomegaly).

Immunization protocols and adoptive transfer experiments. For short-term immunizations, 8- to 12-week-old mice were immunized by i.p injection of srbc (1×10^9), boosted twice (day 15 and day 30), and tissues were analyzed 7 days after the last immunization by cell sorting, molecular analysis, and histology.

For long-term chronic immunizations, mice were immunized by i.p. injection of srbc (1×10^9) followed by sequential injections of srbc every 3 weeks over a 9-month period (Figure 2). Mice were sacrificed on day 7 after the last injection at the peak of the GC response, and tissues were processed for flow cytometry, cell sorting, and molecular analysis.

For adoptive transfer experiments (Figure 3), 6- to 8-week-old recipient C57BL/6 WT mice were immunized once by i.p. injection of srbc (1×10^9) 1 month prior to transfer with sorted EYFP⁺GL7⁺/⁻IgM⁺/⁻ splenocytes from chronically immunized mice (15,000–50,000 cells i.v.). Recipients were then challenged 2 hours after transfer and sac-

rificed 1 week later for flow cytometry, cell sorting, molecular analysis, and/or histology.

Cell staining, flow cytometric analysis, and cell sorting. For mouse cell sorting and flow cytometric analysis, single-cell suspensions from normal or tumoral lymphoid organs (spleen and LNs) were stained with the following antibodies: CD19, IgK, IgM, IgD, GL7, CD38, CD21, CD23, B220, huBCL2, and CD138 in various combinations to delineate the different stages of B cell differentiation. For each sorting experiment using *BCL2*tracer mice in resting or activation mode, B cells were enriched by negative selection using the EasySep Mouse B cell Enrichment Kit (STEMCELL Technologies), stained, and gated on the CD19⁺ pool. IgK, IgM, and IgD⁺ cells define the mature naive B cells, while activated B cells were sorted as CD19⁺GL7⁺ (GC) and CD19⁺GL7⁻IgM⁻IgD⁻ (memory). Plasmablasts (PBs) were isolated from the CD19neg fraction and defined as B220loCD138⁺ cells. Sorting was repeated at least twice for all the mouse strains, but only once for the PB fraction. Alternatively, in retrovirus-based experiments, GC and post-GC B cells were sorted from the spleens of huBCL2 retrovirally transduced *Aid-Cre Rosa-EYFP* mice based on CD19, EYFP, GL7, IgM, IgD, and IgG₁ expression, and the purified cell fractions were subsequently used for adoptive transfer experiments. All antibodies, clone numbers, dilutions, and conjugates of all antibodies used in this study are listed in Supplemental Table 11.

Whole-exome mouse sequencing and analysis. The 50-Mb mouse exome was captured using Agilent SureSelect XT, genome version GRCm38/mm10. Capture libraries were constructed from 1 μg of WGA-amplified DNA from GC and post-GC subsets (BCL2-enriched or control empty vector) and germlines (naive) using the REPLI-g Single Cell Kit (QIAGEN). Enriched exome libraries were multiplexed and sequenced on the Illumina HiSeq 2000 platform to generate 100-bp paired-end reads. All sequence data were quality controlled for read counts, quality values, kmer usage, GC content, and all other relevant parameters within FastQC version 0.10.1 (Babraham Bioinformatics). The DNA sequence was aligned to the mouse genome (UCSC mm10; Dec 2011 release; Genome Reference Consortium GRCh38) using Bowtie2, version 2.1.0 (SourceForge). SAMtools version 0.1.18 mpileup was used (Qphred >30 and mapping quality >30) with VarScan2 version 2.3.2 to call SNVs relative to the mouse reference with the following parameters: variant minimum frequency greater than 5%, VarScan2 *P* value for variant calls (based on Fisher's exact test) less than 0.01, minimum coverage = 20, minimum reads = 3, minimum average quality = 30, and minimum frequency for homozygote = 0.8.

Variant calls were made for all samples in a batch call and exported as a Variant Call Format (VCF) version 4.1 (1000 Genomes) file. Then, variant call refinement was conducted according to the following rules for somatic SNV calls between pairs of GC versus naive fractions and IgMmem versus naive fractions: (a) average Qphred score for reference or variant (or both) greater than 30 for whole-exome sequencing (WES) in naive, GC, and IgMmem fractions; (b) *P* value by Fisher's exact test of less than 0.01 for read counts between naive, GC, or IgMmem fractions and reference or variant; (c) VAF in naive fractions of less than 3%; and (d) GC or IgMmem VAF at least 5% greater than the VAF of the naive fraction. Annotation and variant effects on genes were then conducted using ANNOVAR (version 2013-07-28), and all nonsilent (i.e., nonsynonymous, stopgain, or stoploss) SNVs were selected. Putative somatic variants identified in dbSNP (snp138) were removed from consider-

ation. To identify potential strain-specific (129P2 and C57BL/6NJ) SNPs, data from snp137 (mm9) were compared against our somatic variant loci (mm10 to mm9 converted), and loci in common were excluded. In an effort to control for presumed SNP loci not present in snp137 or snp138, a particular locus was removed if it was in common in any fraction comparison between 2 (or more) mice (B1, B3, and B4). Multiple sources can be attributed to these variant calls, potentially due to genetic drift of the C57BL/6J mouse strain versus the C57BL/6 reference genome. Identified somatic variants and allelic frequencies are displayed in Supplemental Table 5.

Statistics. Results are reported as the mean ± SEM. Significance was evaluated by 2-tailed Student's *t* test. Statistical comparisons were performed by 2-tailed Student's *t* and Mann-Whitney *U* tests using GraphPad Prism software (GraphPad Software). A *P* value of less than 0.05 was considered significant.

Study approval. Written informed consent was obtained from the donors or relatives in accordance with the Declaration of Helsinki and with IRB approval of the French Biomedicine Agency. The collection of human lymphoid samples issued from cardiac surgeries, child routine tonsillectomies, and benign hyperplasia and FLIS was approved by the IRB and ethics committee of CHU Pontchaillou (Rennes, France) (CPP 06/01-567), the Centre Henri Becquerel (Rouen, France), and the Institut Paoli-Calmettes (Marseille, France). Written informed consent was obtained from all patients, and all animal procedures were approved by and performed in accordance with guidelines of the Centre d'Immunologie de Marseille Luminy (CIML).

Acknowledgments

Address correspondence to: Sandrine Roulland, Centre d'Immunologie de Marseille-Luminy, Aix-Marseille University, 13288 Marseille cedex 9, France. Phone: 33.0.491.269.473; E-mail: roulland@ciml.univ-mrs.fr. Or to: Bertrand Nadel, Centre d'Immunologie de Marseille-Luminy, Aix-Marseille Université, 13288 Marseille Cedex 9, France. Phone: 33.0.491.269.466; E-mail: nadel@ciml.univ-mrs.fr.

Stéphanie Sungalee's present address is: European Molecular Biology Laboratory (EMBL), Heidelberg, Germany.

Franziska C. Eberle's present address is: Department of Dermatology, Eberhard Karls University, Tübingen, Germany.

Julie Tellier's present address is: The Walter and Eliza Hall Institute of Medical Research, Parkville, Victoria, Australia.

Rachel Kelly's present address is: Department of Epidemiology, Harvard School of Public Health, Boston, Massachusetts, USA.

1. MacLennan IC. Germinal centers. *Annu Rev Immunol*. 1994;12:117–139.
2. Victora GD, et al. Germinal center dynamics revealed by multiphoton microscopy with a photoactivatable fluorescent reporter. *Cell*. 2010;143(4):592–605.
3. Gitlin AD, Shulman Z, Nussenzweig MC. Clonal selection in the germinal centre by regulated proliferation and hypermutation. *Nature*. 2014;509(7502):637–640.
4. Schwickert TA, Alabyev B, Manser T, Nussenzweig MC. Germinal center reutilization by newly activated B cells. *J Exp Med*. 2009;206(13):2907–2914.
5. Bende RJ, van Maldegem F, Triesscheijn M, Wormhoudt TA, Guijt R, van Noesel CJ. Germinal centers in human lymph nodes contain reactivated memory B cells. *J Exp Med*. 2007;204(11):2655–2665.
6. Dogan I, et al. Multiple layers of B cell memory with different effector functions. *Nat Immunol*. 2009;10(12):1292–1299.
7. Pape KA, Taylor JJ, Maul RW, Gearhart PJ, Jenkins MK. Different B cell populations mediate early and late memory during an endogenous immune response. *Science*. 2011;331(6021):1203–1207.
8. Klein U, Dalla-Favera R. Germinal centres: role in B-cell physiology and malignancy. *Nat*. 2008;8(1):22–33.
9. Roulland S, Faroudi M, Mamessier E, Sungalee S, Salles G, Nadel B. Early steps of follicular lym-

phoma pathogenesis. *Adv Immunol*. 2011;111:1–46.
10. Swerdlow S, et al. *WHO Classification of Tumours of Haematopoietic and Lymphoid Tissues*. 4th ed. Geneva Switzerland: WHO Press; 2008.
11. Cong P, Raffeld M, Teruya-Feldstein J, Sorbara L, Pittaluga S, Jaffe ES. In situ localization of follicular lymphoma: description and analysis by laser capture microdissection. *Blood*. 2002;99(9):3376–3382.
12. Jegalian AG, et al. Follicular lymphoma in situ: clinical implications and comparisons with partial involvement by follicular lymphoma. *Blood*. 2011;118(11):2976–2984.
13. Liu Y, Hernandez AM, Shibata D, Cortopassi GA. BCL2 translocation frequency rises with age in humans. *Proc Natl Acad Sci U S A*. 1994;91(19):8910–8914.
14. Roulland S, et al. Follicular lymphoma-like B cells in healthy individuals: a novel intermediate step in early lymphomagenesis. *J Exp Med*. 2006;203(11):2425–2431.
15. Schuler F, et al. Prevalence and frequency of circulating t(14;18)-MBR translocation carrying cells in healthy individuals. *Int J Cancer*. 2009;124(4):958–963.
16. Hirt C, Dolken G, Janz S, Rabkin CS. Distribution of t(14;18)-positive, putative lymphoma precursor cells among B-cell subsets in healthy individuals. *Br J Haematol*. 2007;138(3):349–353.
17. Bretherick KL, Bu R, Gascoyne RD, Connors

JM, Spinelli JJ, Brooks-Wilson AR. Elevated circulating t(14;18) translocation levels prior to diagnosis of follicular lymphoma. *Blood*. 2010;116(26):6146–6147.
18. Roulland S, et al. t(14;18) Translocation: A predictive blood biomarker for follicular lymphoma. *J Clin Oncol*. 2014;32(13):1347–1355.
19. Carlotti E, et al. Transformation of follicular lymphoma to diffuse large B-cell lymphoma may occur by divergent evolution from a common progenitor cell or by direct evolution from the follicular lymphoma clone. *Blood*. 2009;113(15):3553–3557.
20. Weigert O, et al. Molecular ontogeny of donor-derived follicular lymphomas occurring after hematopoietic cell transplantation. *Cancer Discov*. 2012;2(1):47–55.
21. Agopian J, et al. Agricultural pesticide exposure and the molecular connection to lymphomagenesis. *J Exp Med*. 2009;7(7):1473–1483.
22. Genton C, et al. The Th2 lymphoproliferation developing in Lat(Y136F) mutant mice triggers polyclonal B cell activation and systemic autoimmunity. *J Immunol*. 2006;177(4):2285–2293.
23. Robbiani DF, et al. AID is required for the chromosomal breaks in c-myc that lead to c-myc/IgH translocations. *Cell*. 2008;135(6):1028–1038.
24. Mamessier E, et al. Early lesions of follicular lymphoma: a genetic perspective. *Haematologica*. 2014;99(3):481–488.

25. Schmidt J, et al. Increasing genomic and epigenomic complexity in the clonal evolution from in situ to manifest t(14;18)-positive follicular lymphoma. *Leukemia*. 2014;28(5):1103–1112.

26. Colombat P, et al. Rituximab (anti-CD20 monoclonal antibody) as single first-line therapy for patients with follicular lymphoma with a low tumor burden: clinical and molecular evaluation. *Blood*. 2001;97(1):101–106.

27. Saito M, et al. BCL6 suppression of BCL2 via Miz1 and its disruption in diffuse large B cell lymphoma. *Proc Natl Acad Sci U S A*. 2009;106(27):11294–11299.

28. Nagaoka H, Muramatsu M, Yamamura N, Kinoshita K, Honjo T. Activation-induced deaminase (AID)-directed hypermutation in the immunoglobulin Smu region: implication of AID involvement in a common step of class switch recombination and somatic hypermutation. *J Exp Med*. 2002;195(4):529–534.

29. Seifert M, Kuppers R. Molecular footprints of a germinal center derivation of human IgM+(IgD+) CD27+ B cells and the dynamics of memory B cell generation. *J Exp Med*. 2009;206(12):2659–2669.

30. Lenz G, et al. Aberrant immunoglobulin class switch recombination and switch translocations in activated B cell–like diffuse large B cell lymphoma. *J Exp Med*. 2007;204(3):633–643.

31. Du L, et al. Cernunnos influences human immunoglobulin class switch recombination and may be associated with B cell lymphomagenesis. *J Exp Med*. 2012;209(2):291–305.

32. Mamani-Matsuda M, et al. The human spleen is a major reservoir for long-lived vaccinia virus-specific memory B cells. *Blood*. 2008;111(9):4653–4659.

33. Nunez G, Hockenbery D, McDonnell TJ, Sorensen CM, Korsmeyer SJ. Bcl-2 maintains B cell memory. *Nature*. 1991;353(6339):71–73.

34. Smith KGC, Light A, O'Reilly LA, Ang SM, Strasser A, Tarlinton D. bcl-2 transgene expression inhibits apoptosis in the germinal center and reveals differences in the selection of memory B cells and bone marrow antibody-forming cells. *J Exp Med*. 2000;191(3):475–484.

35. Weigert O, et al. Molecular ontogeny of donor-derived follicular lymphomas occurring after hematopoietic cell transplantation. *Cancer Discov*. 2012;2(1):47–55.

36. Hanahan D, Weinberg RA. Hallmarks of cancer: the next generation. *Cell*. 2011;144(5):646–674.

37. Dave SS, et al. Prediction of survival in follicular lymphoma based on molecular features of tumor-infiltrating immune cells. *N Engl J Med*. 2004;351(21):2159–2169.

38. Tellier J, et al. Human t(14;18)positive germinal center B cells: a new step in follicular lymphoma pathogenesis? *Blood*. 2014;123(22):3462–3465.

39. Pasqualucci L, et al. Genetics of follicular lymphoma transformation. *Cell Rep*. 2014;6(1):130–140.

40. Okosun J, et al. Integrated genomic analysis identifies recurrent mutations and evolution patterns driving the initiation and progression of follicular lymphoma. *Nat Genet*. 2014;46(2):176–181.

41. Kluin PM. Origin and migration of follicular lymphoma cells. *Haematologica*. 2013;98(9):1331–1333.

42. Guglielmi L, et al. The 5'HS4 insulator element is an efficient tool to analyse the transient expression of an Em mu-GFP vector in a transgenic mouse model. *Transgenic Res*. 2005;14(4):361–364.

43. Prinz I, Sansoni A, Kissenpfennig A, Ardouin L, Malissen M, Malissen B. Visualization of the earliest steps of gammadelta T cell development in the adult thymus. *Nat Immunol*. 2006;7(9):995–1003.

44. Coico RF, Bhogal BS, Thorbecke GJ. Relationship of germinal centers in lymphoid tissue to immunologic memory. VI. Transfer of B cell memory with lymph node cells fractionated according to their receptors for peanut agglutinin. *J Immunol*. 1983;131(5):2254–2257.